Progress In Electromagnetics Research M, Vol. 62, 89–98, 2017

MM-Wave Dielectric Parameters of Magnesium Fluoride Glass Wafers

Vladimir B. Yurchenko[1, *], Mehmet Ciydem[1], Marcin L. Gradziel[2], and Lidiya V. Yurchenko[3]

Abstract—We measured millimeter-wave dielectric parameters of magnesium fluoride glass wafers at the room temperature in the frequency band of 75–110 GHz by applying the open resonator technique based on the use of Bragg structures and related multi-layer assemblies. Through the comparison of measured and simulated transmission spectra of various structures, the dielectric constant of magnesium fluoride glass is found as $\varepsilon = 5.50 \pm 0.01$. The estimate for the loss tangent is found to be $\tan\delta = 0.00005$, with a possibility that the actual losses could be smaller than this value.

1. INTRODUCTION

New applications of infrared (IR), terahertz (THz), and millimeter (MM) waves require the use of novel dielectric materials with enhanced chemical, mechanical, and electromagnetic properties. A promising class of materials is the group of fluorides of lithium, calcium, barium, and magnesium. They show exceptional performance when being used as a whispering-gallery-mode resonator [1, 2] and promise to be a perfect dielectric mirror in the systems for generation of ultrashort THz pulses [3] and microwave dynamical chaos [4]. Despite this, dielectric properties of fluorides have not yet been studied in detail. In particular, they have not been extensively measured at microwave frequencies, except for some crystalline materials at cryogenic temperatures [5, 6]. Even less is known about optical properties of amorphous materials (glasses) in the MM-wave band, which covers the frequency range of $f = 30$ GHz to 300 GHz.

The aim of this work is to measure the MM-wave dielectric constant and losses of magnesium fluoride glass wafers in the W frequency band (the frequency range of $f = 75$–110 GHz) by using a Bragg resonator technique.

There are many experimental methods for measuring high-frequency dielectric parameters of materials [7, 8]. Of all available methods, resonant techniques are particularly attractive for high-precision measurements of real and imaginary parts of complex dielectric constant [9–12]. The most impressive results were achieved with high-quality open resonators employing large-area mirrors and providing quality factors (Q factors) exceeding $6 \cdot 10^5$ at the frequencies $f \sim 100$ GHz [9]. Bragg structures could provide an alternative solution where high-Q resonator properties are combined with compactness of the measurement system.

Enhanced sensitivity and accuracy of resonant techniques is achieved due to spatial confinement of electromagnetic wave inside the material under test. The measurement system could be made as a periodic Bragg structure with a resonant "defect layer" of tested material. The layer creates a narrow peak in the transmission band gap of the structure which is sensitive to the dielectric parameters of the

Received 18 August 2017, Accepted 3 November 2017, Scheduled 11 November 2017

* Corresponding author: Vladimir Yurchenko (v.yurchenko.nuim@gmail.com).

[1] Engitek Engineering Technologies Ltd, 197/16 Ceyhun Atif Kansu St., Ankara 06460, Turkey. [2] Department of Experimental Physics, Maynooth University, Maynooth, Ireland. [3] O. Ya. Usikov Institute for Radiophysics and Electronics, National Academy of Sciences of Ukraine, 12 Proskura St., Kharkiv 61185, Ukraine.

layer. The Bragg systems of this kind, though having lower Q-factors as compared to record breaking values reported in [9], are relatively simple for fabrication and sufficient for typical purposes.

2. MAGNESIUM FLUORIDE STRUCTURES AND MM-WAVE MEASUREMENTS

We measured dielectric properties of magnesium fluoride (MgF_2) glass wafers available in the form of thin disks of thickness $t = 0.55\,\text{mm}$ and external diameter $D = 75\,\text{mm}$, supplied by WTS Photonics (China). For making the Bragg structures, we selected a set of wafers of identical thickness $t = 0.550\,\text{mm}$, measured with accuracy of about $\Delta t = \pm 0.001\,\text{mm}$. Thickness was verified across the entire area of each wafer, including the rim area where the spacer rings, which control the air spaces between the wafers, are placed.

We considered four types of structures composed of wafers with or without air spaces between them. The structures of type #1 were tight stacks of wafers with essentially no air spaces between them. The structures of types #2 and #3 were periodic assemblies of wafers separated with air spaces of thickness $a = 0.102\,\text{mm}$ and $v = 0.697\,\text{mm}$, respectively. Finally, the structures of type #4 were Bragg assemblies with a resonant "defect layer" which is created by making the air spaces around the central wafer of twice greater thickness $2v = 1.384\,\text{mm}$ than the air spaces $v = 0.697\,\text{mm}$ in the periodic parts of structure (Bragg mirrors).

The structures #1 are denoted as $m1$, $m2$, etc., where m signifies the MgF_2 wafer, and numerals are the numbers of wafers in the stack. The structures #2 and #3 are denoted as $Nma - m$ and $Nmv - m$, respectively, where N is the number of air spaces, and $N + 1$ is the number of wafers. Finally, the structures #4 are denoted as $Kmv - vmv - Kvm$ where the number of wafers is $N = 2K + 1$.

The spacer rings controlling the air spaces were cut by electrochemical etching of gauged stainless steel and brass sheets of nominal thickness $a = 0.10\,\text{mm}$ and $v = 0.70\,\text{mm}$, respectively. Multiple measurements of thickness made at various points on separate rings and stacks of rings indicate variations of a and v in the range from about $a = 0.100\,\text{mm}$ and $v = 0.695\,\text{mm}$ to the values of $a = 0.102\,\text{mm}$ and $v = 0.697\,\text{mm}$ specified above. Since the air spaces are controlled by the maxima of thickness of spacer rings, the latter are the effective values to be used in simulations below.

MM-wave measurements were made using a Vector Network Analyzer (VNA) quasi-optical bench facility at the Maynooth University Department of Experimental Physics (Maynooth, Ireland). The VNA (R&S ZVA24) is equipped with frequency extension heads (ZVA-Z110) for W-band operation. The bench is furnished with custom split-step dual-aspheric MM-wave Fresnel lenses [13] which refocus nearly Gaussian beams of conical corrugated horns [14] fed by the VNA heads as shown in Figure 2(b) in [15]. The lenses create near-Gaussian beams of the waist radius $w_A = 24\,\text{mm}$ at the aperture of stainless-steel holder carrying a Bragg structure inside (the aperture radius is $R_A = 34\,\text{mm}$) [15]. The axial positions of the VNA heads and lenses z_n ($n = 1{-}4$, Figure 1) were computer controlled using Zaber linear actuators. This allowed us to perform standing wave averaging using repeated measurements with different small offsets of z_n.

The procedure of z-averaging of spectral data measured at different offsets of z_n (e.g., using 121 points in the range of two wavelengths around reference positions) eliminates the oscillatory effects of standing waves on transmission and reflection spectra. It is an essential development as compared to

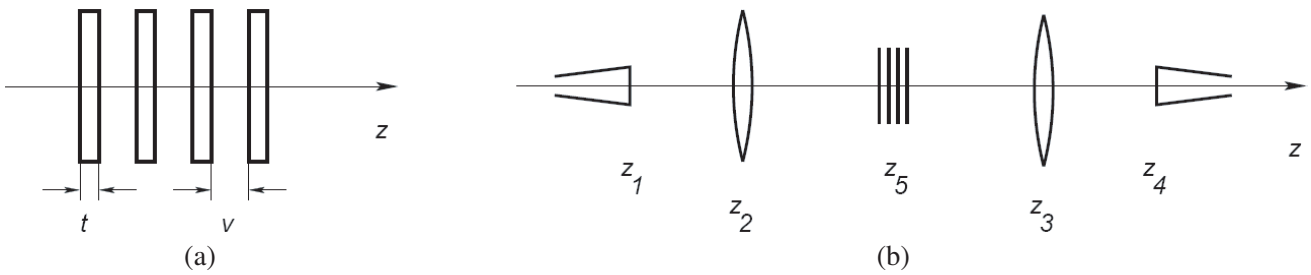

Figure 1. Schematic diagrams of (a) Bragg mirror and (b) measurement setup using VNA feed horns at z_1 and z_4, dielectric lenses at z_2 and z_3, and a Bragg structure at z_5.

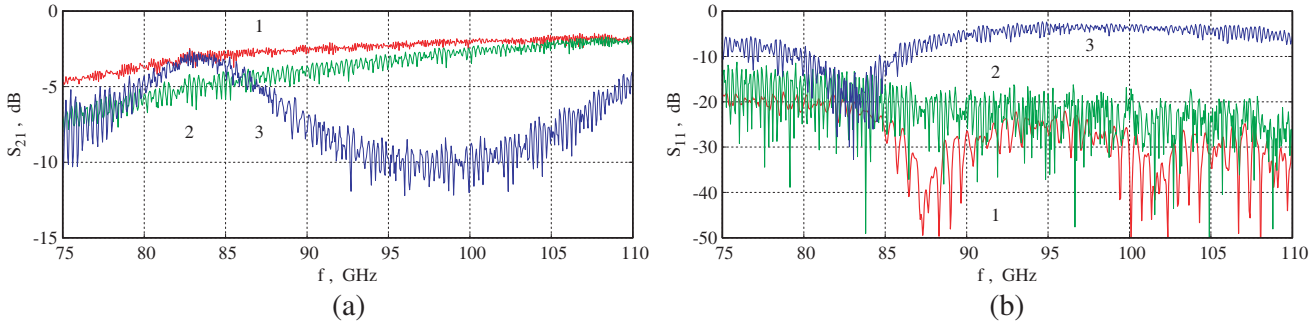

Figure 2. (a) Transmission and (b) reflection spectra recorded by the VNA in the case of (1) beam incident on the aperture of (a) an empty holder and (b) a holder with an absorber (reference data), (2) a single MgF_2 wafer fixed in the holder ($m1$ structure), and (3) a Bragg structure of 5 MgF_2 wafers with 4 air spaces of thickness $a = 0.102$ mm ($4ma - m$ structure).

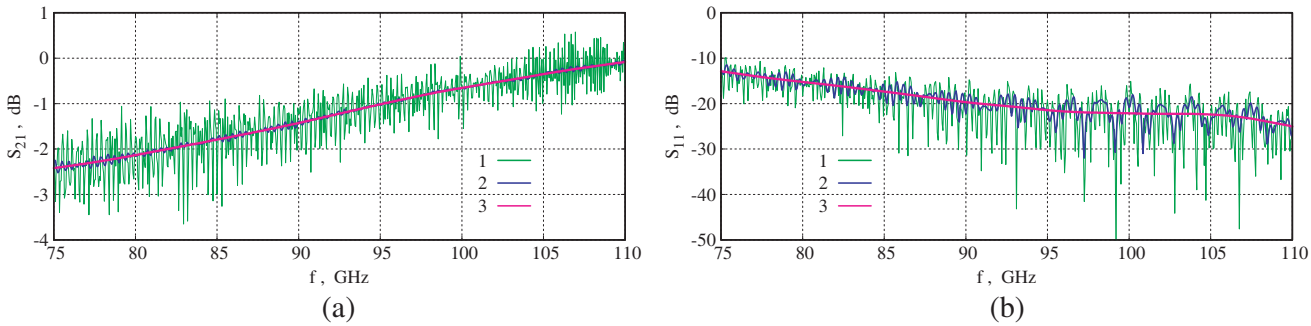

Figure 3. (a) Transmission and (b) reflection spectra of $m1$ structure with account of reference when using (1) original VNA data, (2) processed data after filtering off the standing waves, and (3) final data after residual smoothing.

earlier measurements [15] where spectral curves for the comparison with simulations were taken at the fixed positions of quasi-optical components. The development increases the accuracy of the technique that makes it possible to use the method for characterization of ultra-low-loss dielectric materials.

Figures 2–7 show the MM-wave transmission and reflection spectra measured for a few types of Bragg structures made of MgF_2 glass wafers. Figure 2 presents the original data recorded at reference position of the VNA heads and lenses. It shows typical spectra measured with (1) an empty holder and a holder with an absorber (the results used as the reference data), (2) a single MgF_2 wafer ($m1$ structure of type #1), and (3) a regular Bragg structure $4ma - m$ (an example of structure of type #2).

Figures 3 and 4 show the results of numerical processing of raw data presented in Figure 2. The processing includes the account of reference signals presented by curves 1 in Figure 2, filtering out the oscillatory effects emerging on spectral curves due to the standing waves formed, mainly, between the transmitter and receiver horns, and smoothing the residual rippling on spectral curves that remains after removing the standing wave effects. This set of figures demonstrates how well the actual transmission and reflection spectra can be recovered from the original records of S_{21} and S_{11} signals (the scattering matrix coefficients) captured by the VNA, which were affected by artifacts attributable to our quasi-optical bench.

Figures 5–7 show the MM-wave spectra measured for typical representative structures including the wafer stacks of type #1 ($m1$, $m3$, and $m5$ structures), the Bragg structures of types #2 and #3 ($2ma - m$, $3ma - m$, and $4ma - m$ cases with $a = 0.102$ mm compared to $1mv - m$ and $3mv - m$ cases with $v = 0.697$ mm, respectively), and the "defect layer" structure of type #4 ($2mv - vmv - 2vm$ with $v = 0.697$ mm). The measurements were made in the temperature range of $T = 20.6$–22.6°C.

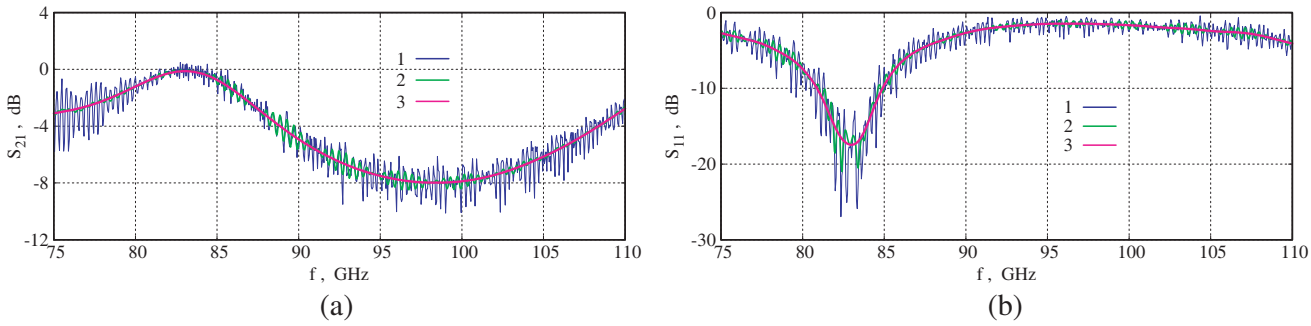

Figure 4. (a) Transmission and (b) reflection spectra of $4ma - m$ structure with account of reference when using (1) original VNA data, (2) processed data after filtering off the standing waves, and (3) final data after residual smoothing.

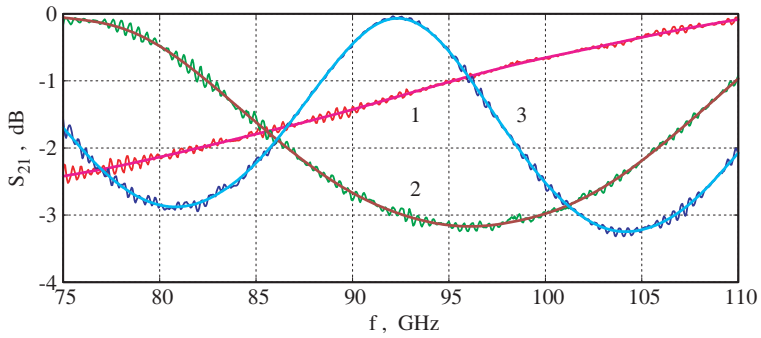

Figure 5. Measured transmission spectra of (1) $m1$, (2) $m3$, and (3) $m5$ tight MgF_2 stack structures after filtering off the standing waves (thin curves with rippling) and final residual smoothing (solid curves), all with account of reference.

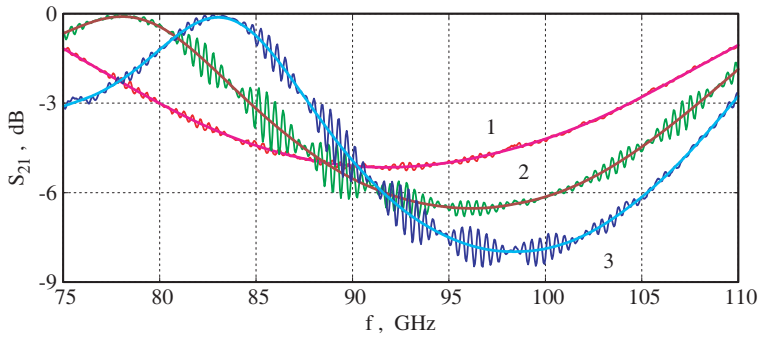

Figure 6. Measured transmission spectra of (1) $2ma - m$, (2) $3ma - m$, and (3) $4ma - m$ Bragg structures with $a = 0.102$ mm air spaces after filtering off the standing waves (thin curves with rippling) and final residual smoothing (solid curves), all with account of reference.

The analysis of reference data taken under various conditions (an empty holder, a beam with no holder, different sets of ring spacers with no wafers, renewed VNA calibrations) allowed us to identify the level of accuracy of spectral measurements available in the cases of interest. Specifically, discrepancies between reference transmission curves S_{21} for different settings of a holder with no wafers (an example is curve 1 in Figure 2) are about 0.1 dB. At the same time, the average transmission through the aperture of an empty holder is about 0.25 dB below the free-space beam transmission measured with no holder (the difference decreases from 0.4 dB at 75 GHz to 0.1 dB at 110 GHz).

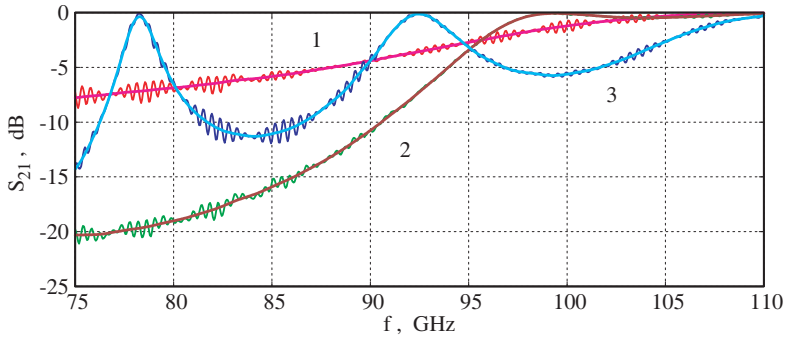

Figure 7. Measured transmission spectra of (1) $1mv - m$, (2) $3mv - m$, and (3) $2mv - vmv - 2vm$ Bragg structures with $v = 0.697$ mm air spaces after filtering off the standing waves (thin curves with rippling) and final residual smoothing (solid curves), all with account of reference.

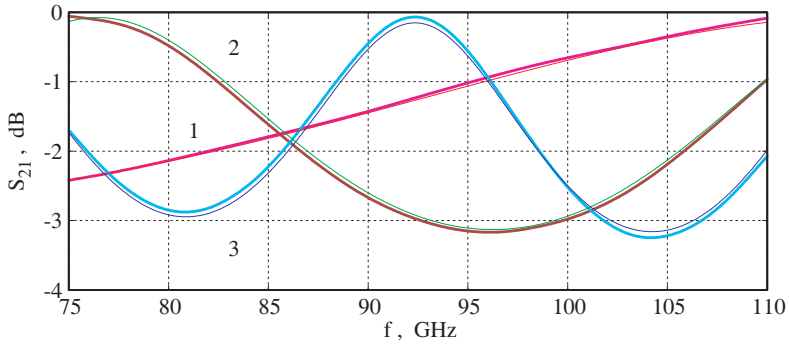

Figure 8. Measured and simulated transmission spectra (solid and thin curves, respectively) of (1) $m1$, (2) $m3$, and (3) $m5$ tight MgF_2 stack structures (air spaces $u_3 = 0.012$ mm and $u_5 = 0.006$ mm are used in $m3$ and $m5$ simulations, respectively).

3. NUMERICAL SIMULATIONS AND EXTRACTION OF DIELECTRIC PARAMETERS

Simulations of MM-wave propagation through multi-layer structures are based on the plane-wave transmission matrix approach [15, 16] extended for spatially-limited vector electromagnetic beams. Plane-wave transmission matrix simulations are straightforward. For computing spatially-limited beam propagation, we use a vector plane-wave spectrum representation of beams proposed in [17, 18].

Assuming that the incident beam is linearly polarized along the vertical x-axis and has an axially symmetric plane-wavefront Gaussian profile of the E_x electric field component within the holder aperture (zero field is assumed outside the aperture), we recovered all the components of electric and magnetic fields of partial plane waves satisfying Maxwell's equations. Then, propagating the partial plane waves through the structure and using Fourier transform for recovering transmitted and reflected beams, we simulated propagation and reflection of beams by a multi-layer structure.

As the final step, transmission and reflection signals are evaluated as the scalar products of complex amplitudes of transformed beam fields and receiver beam patterns taken within the holder aperture. In this way, we could account, approximately, for the effects of holder aperture diameter on the spectra being considered. These simulations were employed for the estimation of beamwidth effects and their comparison with the effects of dielectric losses.

For the recovery of dielectric parameters of wafers, we used all kinds of multi-layer structures specified above (Figures 8–11). When considering a single wafer, we observe a small effect, which is not so good for the accurate extraction of dielectric parameters (Figure 8). Using a stack of wafers increases

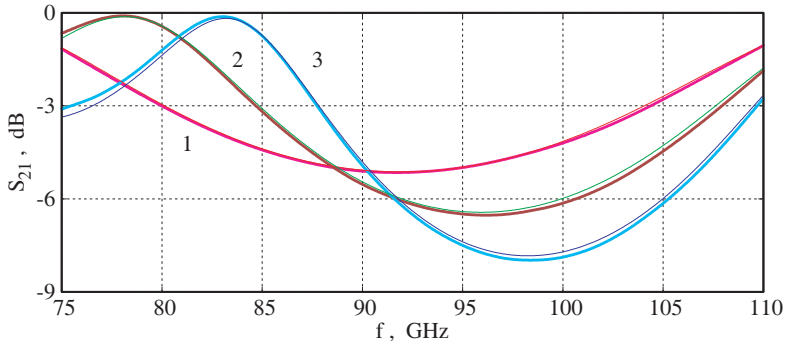

Figure 9. Measured and simulated transmission spectra (solid and thin curves, respectively) of (1) $2ma - m$, (2) $3ma - m$, and (3) $4ma - m$ Bragg structures with $a = 0.102$ mm air spaces.

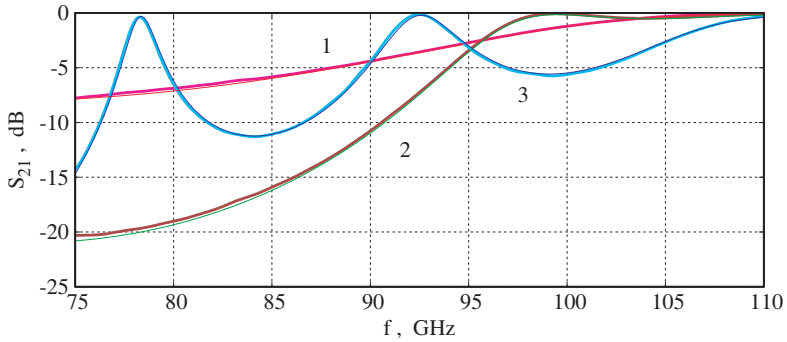

Figure 10. Measured and simulated transmission spectra (solid and thin curves, respectively) of (1) $1mv - m$, (2) $3mv - m$, and (3) $2mv - vmv - 2vm$ Bragg structures with $v = 0.697$ mm air spaces.

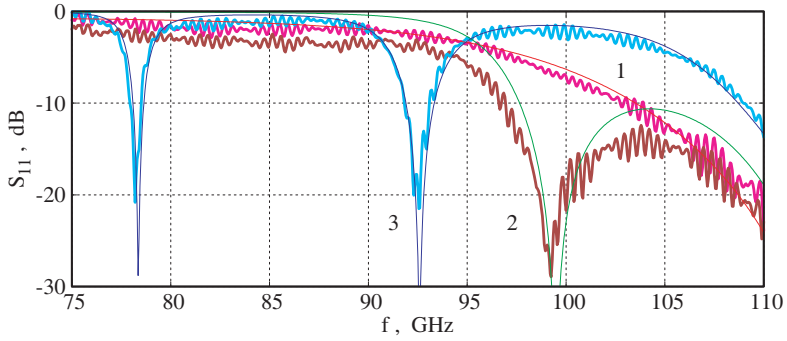

Figure 11. Measured and simulated reflection spectra (solid and thin curves, respectively) of (1) $1mv - m$, (2) $3mv - m$, and (3) $2mv - vmv - 2vm$ Bragg structures with $v = 0.697$ mm air spaces.

the wave coupling to the wafers that, in turn, increases the measurement accuracy. In practice, though, there are minor uncontrollable spaces between wafers due to non-ideal flatness of their surfaces. These spaces produce a noticeable effect on transmission and reflection spectra. As a result, the data in these cases become less reliable for the accurate parameter extraction than expected.

Bragg structures with air spaces of greater thickness (e.g., approaching a quarter-wavelength value) produce characteristic features on spectral curves which are better suited for evaluation of dielectric parameters. In this case, the mean values of air spaces are under better control, and the spectra are less sensitive to the same inaccuracy of individual layers. The use of structures of different types provides a set of conditions for sufficiently accurate extraction of parameters. The consistency of all measured

and simulated data serves as a test of accuracy of the entire procedure.

The results of simulations and measurements are presented in Figures 8–11. Simulations are performed using the model of plane wave incidence at the wafer dielectric constant $\varepsilon = 5.50$, loss tangent $\tan\delta = 0.002$, and wafer thickness $t = 0.550\,\text{mm}$. The best match between measured and simulated curves is achieved by varying the air spaces between wafers. In all the structures of #2, #3, and #4, the best match is obtained at the air spaces $a = 0.102\,\text{mm}$ and $v = 0.697\,\text{mm}$. This confirms the values expected above. In the case of structure #1, if no spaces are used, the match is not so good, but if minor spaces are introduced, the match is improved (see Figure 8).

For all the structures considered, the difference between measured and simulated transmission spectra is, typically, below 0.2 dB that is about the accuracy limit of our data. Computing transmission spectra at the given uncertainty of wafer thickness ($\Delta t = 0.001\,\text{mm}$), we find the accuracy of dielectric constant as $\Delta\varepsilon = \pm 0.01$. The reflection spectra are less suitable for quantitative analysis since they are more sensitive to various imperfections (e.g., misalignments, see curve 2 in Figure 11). The reflection curves are nonetheless useful for checking all data for consistency.

Estimates of absorption losses can be improved by using the structures with transmission peaks in the middle of band gap that covers the frequency range $f = 75$–$110\,\text{GHz}$. Available MgF_2 wafers are not suitable for making structures of this type, but when being used as the defect layers in the quartz-based assemblies as those in [15], they produce transmission spectra as required (Figures 12 and 13). Because of different materials, many layers, and uncertainty of each layer thickness, the estimate of material dielectric constant in these structures is less reliable. At the same time, due to enhanced sensitivity of transmission peaks to the absorption in the resonant MgF_2 layers, transmission peaks provide a good measure of MgF_2 loss tangent even if the latter is small as compared to the loss tangent of quartz.

Firstly, using the structures with quartz wafers, we made an estimate of the fused quartz dielectric constant $\varepsilon_q = 3.80$ and the loss tangent $\tan\delta_q = 0.001$. Then, considering various structures with insertion of MgF_2 resonant layers, we estimated the parameters of MgF_2 wafers. For the best fitting of measured and simulated spectra, we adjusted the values of air spaces used in simulations while keeping them consistent with measured thickness of wafers, spacer rings, and entire structures. For greater robustness of results, the cases of particular interest were those when the insertion of MgF_2 layers created a few transmission peaks which are more difficult to reproduce in the same simulation.

Figures 12 and 13 show an example of measured and simulated spectra for the MgF_2 enhanced structure of the kind $5qv{-}tmsmsmsmt{-}5vq$ (structure #5) where q denotes the fused quartz wafers, and s, t, and v signify various air spaces (the relevant values of thickness are $q = 0.497\,\text{mm}$, $s = 0.125\,\text{mm}$, $t = 0.916\,\text{mm}$, and $v = 0.502\,\text{mm}$ as initially measured and, in the case of air spaces, later adjusted in the process of fitting). The best fitting (curve 1 in Figures 12 and 13) is achieved when the MgF_2 loss tangent is chosen to be $\tan\delta = 0.0001$ at the value of dielectric constant $\varepsilon = 5.50$ (the loss tangent of quartz is accepted to be $\tan\delta_q = 0.001$ as found above). The estimate assumes no other transmission losses arising due to imperfections of structure such as nonuniform thickness and roughness of wafers, tilt of adjacent wafers, finite beam width, etc. Increase of $\tan\delta$ to $2 \cdot 10^{-4}$ and $5 \cdot 10^{-4}$ reduces the

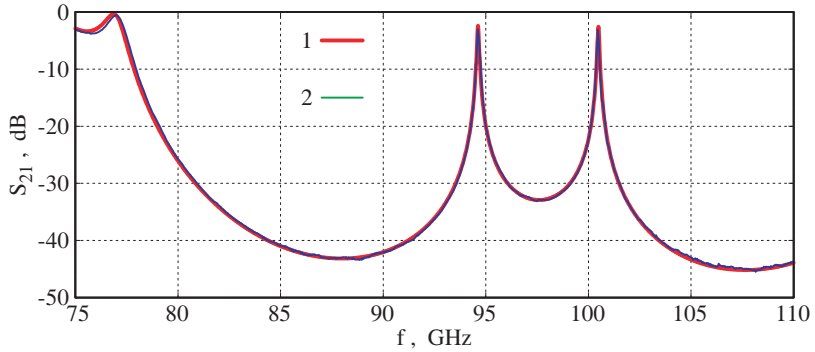

Figure 12. Transmission spectrum of enhanced structure #5 with respect to reference (curves 1 and 2 show simulation and measurement results, respectively).

transmission peak by noticeable 0.3 dB and 1 dB, respectively, whereas decrease to $1 \cdot 10^{-5}$ and further to zero makes little effect (the peak is limited by quartz losses at the level of -2.1 dB).

With no absorption losses, transmission peaks in the ideal structures would reach the level of $S_{21} = 0$ dB. Typical imperfections reduce the peaks as observed in experiments even if no absorption occurs. As an example, curve 2 in Figure 13 shows the effect of random variation of thickness of m and q wafers across the area of each wafer with standard deviation $\delta m = \delta q = 0.2$ μm in case of no absorption (the value of 0.3 μm would further reduce the peak by more than 1 dB). A similar effect arises when a tilt is introduced in an ideal structure so that one of the air spaces t linearly increases from $t = 0.911$ mm to $t = 0.921$ mm across the wafer diameter (the Gaussian beam of the waist radius $w_A = 24$ mm is used in this estimate). Wafer non-flatness also contributes to this effect.

Applying the beam propagation model, we made an estimate of the beamwidth effects (curves 3 and 4 in Figure 13). If the actual beam profile created by lenses [13] is introduced, the beam model applied to an empty holder reproduces the reference curves recorded in the experiments. The mismatch of reference measurements and simulations is about 0.2 dB, which is the same as the discrepancy between different measurements of reference signals.

Using the beam model in case of no absorption in structures of #1 to #4, we obtain transmission spectra similar to those shown in Figures 8–10, which have the same level of mismatch of 0.2 dB with experimental data. In these structures, the beam effect is comparable to the effect of losses computed in the plane wave propagation model at $\tan\delta = 0.002$.

In a similar way, curve 3 in Figure 13 shows the beam effect with no absorption in the MgF_2 enhanced quartz structure #5. In this structure, due to narrow transmission peaks and enhanced sensitivity to the material parameters, the use of beam propagation model is essential. The beam effect is comparable here to the effect of absorption at smaller values of losses.

Curve 4 shows the best fit of the peak magnitude of measured and simulated spectra obtained at the loss tangents of MgF_2 and quartz wafers $\tan\delta = 5 \cdot 10^{-5}$ and $\tan\delta_q = 5 \cdot 10^{-4}$, respectively. We consider these values as the most representative for the given structures (the estimate of $\tan\delta_q$ is also improved in quartz structures when using the beam propagation model). As for the minor shift of transmission peak to the higher frequencies caused by the beam components at oblique incidence, it is easily compensated, e.g., by choosing the air spacer $t = 0.917$ mm instead of $t = 0.916$ mm, with both values satisfying the measurements of total structure thickness at the accuracy of ± 1 μm.

The comparison of absorption losses and imperfection effects shows that the decrease of transmission peaks observed in the experiments may arise due to imperfections rather than caused by the absorption in the material. It means that the loss tangent of MgF_2 wafers could, in fact, be smaller than the upper limit of $\tan\delta = 5 \cdot 10^{-5}$ recovered above. So, the structures with lower level of imperfections are needed for the measurement of absorption losses in ultra-low-loss materials in this approach.

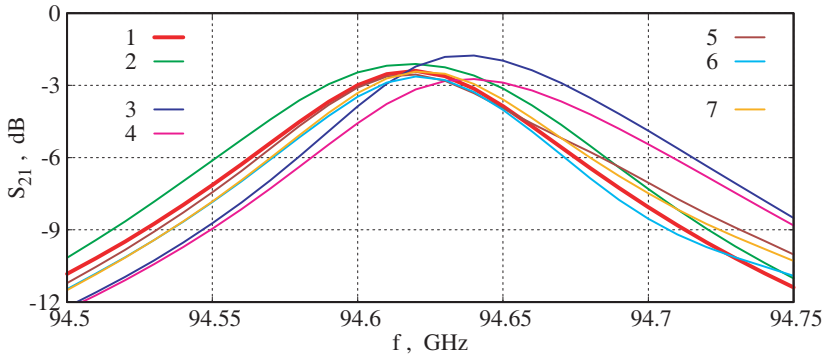

Figure 13. Transmission spectrum of enhanced structure #5 with respect to reference at the first resonant peak ($f = 94.62$ GHz, $Q = 950$). Curves 1 to 4 show simulation results assuming the only imperfections to be (1) the absorption, (2) the roughness of wafers, (3) the beam incidence at finite beam width, and (4) the beam incidence along with absorption, respectively, whereas curves 5 to 7 show the measurement results obtained at a few different re-positionings of the same structure.

4. CONCLUSIONS

In this work, we measured the MM-wave dielectric parameters of magnesium fluoride glass wafers in the W frequency band by applying the resonator technique based on the use of Bragg structures and related multi-layer assemblies. We measured MM-wave transmission and reflection spectra of a few types of structures including tight stacks of wafers, sets of periodic Bragg assemblies, and assemblies with resonant "defect layer" sub-structures, which demonstrate an enhanced sensitivity to the wafer dielectric parameters. The measured spectra were compared with simulation results obtained for the same structures by using the transmission matrix approach implemented in both the plane wave approximation and the beam propagation model.

Based on the analysis of the measured and simulated data obtained for the variety of structures, the dielectric constant of magnesium fluoride glass at the room temperature $T \approx 20°\mathrm{C}$ in the frequency band of $f = 75$–$110\,\mathrm{GHz}$ is found to be $\varepsilon = 5.50 \pm 0.01$ that is consistent with data published for crystalline materials [5, 6]. The estimate for the MgF_2 loss tangent is found to be $\tan\delta = 5 \cdot 10^{-5}$, with a possibility that the actual loss tangent could be smaller (this is also consistent with data obtained for the crystalline MgF_2 at frequencies 9.2 and 20.5 GHz [6]).

ACKNOWLEDGMENT

The research has partially been supported by The Scientific and Technological Research Council of Turkey (TUBITAK) through the 2236 Co-Funded Brain Circulation Scheme ("Co-Circulation"). The VNA laboratory at Maynooth University Department of Experimental Physics was originally funded by Science Foundation Ireland.

REFERENCES

1. Lin, G., S. Diallo, R. Henriet, M. Jacquot, and Y. K. Chembo, "Barium fluoride whispering-gallery-mode disk-resonator with one billion quality-factor," *Opt. Lett.*, Vol. 20, 6009–6012, 2014.
2. Tavernier, H., P. Salzenstein, K. Volyanskiy, Y. K. Chembo, and L. Larger, "Magnesium fluoride whispering gallery mode disk-resonators for microwave photonics applications," *IEEE Photonics Technol. Lett.*, Vol. 22, 1629–1631, 2010.
3. Yurchenko, L. and V. Yurchenko, "Self-generation of ultra-short pulses in a cavity with a dielectric mirror excited by an array of active THz devices," *8th Intl. Conf. on Terahertz Electronics*, 49–52, Darmstadt, Germany, Sept. 28–29, 2000.
4. Yurchenko, L. V. and V. B. Yurchenko, "Analysis of the dynamical chaos in a cavity with an array of active devices," *12th Intl. Conf. on Microwaves and Radar. MIKON-98. Conf. Proc. (IEEE Cat. No.98EX195)*, Vol. 3, 723–727, Krakow, May 20–22, 1998.
5. Geyer, R. G., J. Baker-Jarvis, and J. Krupka, "Variable-temperature microwave dielectric properties of singlecrystal fluorides," *Developments in Dielectric Materials and Electronic Devices*, Vol. 167, Eds. K. M. Nair, R. Guo, A. S. Bhalla, S. I. Hirano, D. Suvorov; *Proc. 106th Annual Meeting of the Am. Ceramic Soc.*, 51–55, 2004.
6. Jacob, M. V., J. Mazierska, and J. Krupka, "Low temperature complex permittivity of MgF_2 at microwave frequencies from $TE_{01\delta}$ modes," *APMC-2005 Asia-Pacific Microwave Conf. Proc.*, Vol. 5, paper 5, Suzhou, China, Dec. 4–7, 2005.
7. Clarke, R. N., A. P. Gregory, D. Cannell, M. Patrick, S. Wylie, I. Youngs, and G. Hill, *A Guide to the Characterisation of Dielectric Materials at RF and Microwave Frequencies*, NPL, Teddington, 2003.
8. Baker-Jarvis, J., M. D. Janezic, B. F. Riddle, R. T. Johnk, P. Kabos, C. L. Holloway, R. G. Geyer, and C. A. Grosvenor, *Measuring the Permittivity and Permiability of Lossy Materials: Solids, Liquids, Metals, Building Materials, and Negative-Index Materials*, NIST, Boulder, CO, 2005.
9. Krupnov, A. F., V. N. Markov, G. Y. Golubyatnikov, I. I. Leonov, Y. N. Konoplev, and V. V. Parshin, "Ultra-low absorption measurement in dielectrics in millimeter- and submillimeter-wave range," *IEEE Trans. Microw. Theory Tech.*, Vol. 47, 284–289, 1999.

10. Krupka, J., "Frequency domain complex permittivity measurements at microwave frequencies," *Meas. Sci. Technol.*, Vol. 17, R55–R70, 2006.
11. Egorov, V. N., "Resonance methods for microwave studies of dielectrics (review)," *Instrum. Exp. Tech.*, Vol. 50, 143–175, 2007.
12. Yurchenko, V. B., "High-Q reflection notch method for mm-wave measurements of large dielectric losses using a stack resonator: Analysis and simulations," *Progress In Electromagnetics Research M*, Vol. 24, 265–279, 2012.
13. Yurchenko, V. B., M. Ciydem, M. Gradziel, J. A. Murphy, and A. Altintas, "Double-sided split-step mm-wave Fresnel lenses: Fabrication and focal field measurements," *J. Europ. Opt. Soc. Rap. Public.*, Vol. 9, 14007–5, 2014.
14. Murphy, J. A., T. Peacocke, B. Maffei, et al., "Multi-mode horn design and beam characteristics for the Planck satellite," *J. Inst.*, Vol. 5, No. 4, T04001–24, 2010.
15. Yurchenko, V., M. Ciydem, M. Gradziel, A. Murphy, and A. Altintas, "Light-controlled photonics-based mm-wave beam switch," *Optics Express*, Vol. 24, 16471–16478, 2016.
16. Born, M. and E. Wolf, *Principles of Optics*, 7th Edition, Cambridge University Press, Cambridge, 2003.
17. Guo, H., J. Chen, and S. Zhuang, "Vector plane wave spectrum of an arbitrary polarized electromagnetic wave," *Optics Express*, Vol. 14, 2095–2100, 2006.
18. Zhou, G., X. Chu, and J. Zheng, "Analytical structure of an apertured vector Gaussian beam in the far field," *Optics Commun.*, Vol. 281, 1929–1934, 2008.